Molecular and Cellular Neuroscience 128 (2024) 103918

Contents lists available at ScienceDirect

Molecular and Cellular Neuroscience

journal homepage: www.elsevier.com/locate/ymcne

A neural mass model for disturbance of alpha rhythm in the minimal hepatic encephalopathy

Jiangling Song [a], M. Brandon Westover [b], Rui Zhang [a,*]

[a] The Medical Big Data Research Center, Northwest University, Xi'an, China
[b] Department of Neurology, Massachusetts General Hospital, Harvard Medical School, Boston, USA

ARTICLE INFO

Keywords:
Minimal hepatic encephalopathy
Neural mass model
Disturbance of alpha waves
Astrocyte-neuronal communication
Sensitivity analysis

ABSTRACT

One of the early markers of minimal hepatic encephalopathy (MHE) is the disruption of alpha rhythm observed in electroencephalogram (EEG) signals. However, the underlying mechanisms responsible for this occurrence remain poorly understood. To address this gap, we develop a novel biophysical model MHE-AWD-NCM, encompassing the communication dynamics between a cortical neuron population (CNP) and an astrocyte population (AP), aimed at investigating the relationship between alpha wave disturbance (AWD) and mechanistical principles, specifically concerning astrocyte-neuronal communication in the context of MHE. In addition, we introduce the concepts of peak power density and peak frequency within the alpha band as quantitative measures of AWD. Our model faithfully reproduces the characteristic EEG phenomenology during MHE and shows how impairments of communication between CNP and AP could promote AWD. The results suggest that the disruptions in feedback neurotransmission from AP to CNP, along with the inhibition of GABA uptake by AP from the extracellular space, contribute to the observed AWD. Moreover, we found that the variation of external excitatory stimuli on CNP may play a key role in AWD in MHE. Finally, the sensitivity analysis is also performed to assess the relative significance of above factors in influencing AWD. Our findings align with the physiological observations and provide a more comprehensive understanding of the complex interplay of astrocyte-neuronal communication that underlies the AWD observed in MHE, which potentially may help to explore the targeted therapeutic interventions for the early stage of hepatic encephalopathy.

1. Introduction

Hepatic encephalopathy (HE) is a spectrum of neuropsychiatric abnormalities associated with liver dysfunction, which is a significant complication in most patients with liver cirrhosis. It encompasses a wide range of neurological symptoms that exhibit varying degrees of severity and impacts a range of functions, including psychomotor abilities, intellectual faculties, cognitive processes, emotional responses, behavioral patterns, fine motor skills, and more.

HE can be divided into five stages based on clinical symptoms or etiology, ranging from grade 0 to grade 4. The minimal hepatic encephalopathy (MHE) or grade 0 HE is located at the beginning of this spectrum and was formerly known as subclinical or latent hepatic encephalopathy. The risk of progression from grade 0 (MHE) to grade 4 is significant, with increased mortality and hospitalization rates for patients. Accurate assessment of HE in its initial stage (i.e., MHE) holds the potential to enable the implementation of suitable intervention strategies, which helps prevent the progression of HE to more severe stages. Such proactive measures could have substantial implications for enhancing the quality and efficacy of treatment, thereby contributing to improved outcomes for affected individuals.

The increasing evidence have shown that the presence of alpha oscillation disturbance in the electroencephalogram (EEG) is a hallmark of MHE (Amodio and Montagnese, 2015). In recent study, Nikhilkumar et al. explored the correlation between MHE and EEG changes, in which all cases were compared with an equal number of healthy controls (Patel et al., 2019). They found that the mean frequency of alpha waves in MHE patients is statistically significant lower than that in healthy controls. This situation is named as "slowing of alpha waves" in their work, which can be used as supportive evidence and for monitoring of MHE (Garnier et al., 2016b). Han et al. found that lower alpha relative power in patients with MHE than in patients without MHE (Han et al., 2020). In the work of Zhang et al., they also found significant decreasing spectral power densities of the alpha oscillations in the HE sub-group (Zhang

* Corresponding author.
E-mail address: rzhang@nwu.edu.cn (R. Zhang).

https://doi.org/10.1016/j.mcn.2024.103918
Received 27 November 2023; Received in revised form 18 January 2024; Accepted 21 January 2024
Available online 1 February 2024

et al., 2022). However, the neural correlates of such abnormal EEG phenomenon are poorly understood. The further studies on the disturbance of alpha waves, especially regarding pathological mechanisms, are significant for deep understanding the early stages of HE (i.e., MHE) and preventing its progression and deterioration.

The pathogenesis of HE remains unclear, but it is widely accepted that the accumulation of ammonia plays a pivotal role in its pathophysiology. Recent studies have shed light on the central role of astrocytes in the pathogenesis of HE, which are critical components of the blood-brain barrier as they communicate directly with neurons (Häussinger et al., 2021; Prakash and Mullen, 2010; Ciećko-Michalska et al., 2012). The alterations related to astrocytes due to HE-relevant factors impair the "astrocytic-neuronal communication" which disturbs oscillatory networks in brain as reflected by the symptoms of HE (May, 2012; Häussinger and Görg, 2019). And in work of (Butz et al., 2013), it is pointed that the emergence of disturbances of oscillatory brain activity precedes the development of HE symptoms after a cascade of complex events, where an important one is disturbances of astrocyte-neuronal communication. However, it is not yet understood how this mechanism relates to the observed disturbance of alpha waves in the early stage of HE. Therefore, the primary objective of this study is to delve into the mechanistic details associated with astrocyte-neuronal communication concerning the disruption of alpha waves (specifically, the reduction in frequency and power spectral density) observed in MHE.

Neural computational modeling is a rapidly growing research area that has proven to be effective in the biomedical field. It allows for the analysis and comprehension of observed EEG phenomena, testing of mechanistic hypotheses, and prediction of system behaviors over time and/or space (Shayegh et al., 2013; Bhattacharya et al., 2011; Li et al., 2020). The microscopic and mesoscopic modeling approaches are developed according to the level of biological organization to be modeled. The former approach mainly focuses on characterizing detailed activity for each individual neuron, while the latter approach focuses more on characterizing average activity for a population of neurons (or neural mass). Compared to microscopic models, mesoscopic models are an essential tool for comprehending the behavior of neural systems at a level of abstraction that is both biologically plausible and computationally feasible. As a result of this recognition, there has been a growing interest in studying mesoscopic models to investigate physiological and pathological phenomena. Here, the typical one is "Liley model", which is proposed by Liley in 1997 to clarify the genesis of alpha rhythms in the mammalian brain (Liley, 1997). Following this, a series of modifications to the Liley model were proposed and applied in an attempt to explain the underlying mechanisms of various physiopathological states. For example, Bojak et al. incorporated a slow process of synaptic resource into the Liley model and explored the emergence of spatially heterogeneous burst suppression during deep anesthesia (Bojak et al., 2015). Hartoyo et al. inferred the mechanisms underlying alpha blocking by fitting the Liley model to EEG spectra from 82 different individuals (Hartoyo et al., 2020).

In our recent work, we integrated three known mechanisms underlying acute HE (AHE) into the Liley model to construct a new computational model NCM-AHE, which is applied to explain the emergency of triphasic waves (TPWs) in AHE EEGs (Song et al., 2019). Inspired by our previous work, the NCM-AHE is taken as the fundamental model in this work to investigate the mechanistic details of alpha wave disturbance (AWD) related to astrocyte-neuronal communication in the MHE. A novel mathematical model MHE-AWD-NCM that encompasses the communication dynamics between astrocyte and neuronal populations is constructed firstly, building upon our previously established NCM-AHE model. It comprises two pathways: feedforward communication originating from the cortical neuron population (CNP) and targeting the astrocyte population (AP), as well as feedback communication from the AP back to the CNP. In addition, we introduce the concepts of peak power density and peak frequency within the alpha band as quantitative measures of AWD. These metrics enable us to investigate the impact of key model parameters on the disturbance of alpha waves in MHE. Subsequently, sensitivity analysis is performed to assess the relative significance of various parameters in influencing alpha wave disruptions in the context of MHE.

2. Materials and methods

2.1. The computational model of HE

The neural computational model of acute HE (NCM-AHE) is an electrocortical model proposed in our previous work to investigate the relationship between the frequency of triphasic waves (TPWs) observed in real AHE-EEGs and the underlying mechanisms of acute HE (Song et al., 2019).

The NCM-AHE is governed by the interaction of two cortical neuron populations: an excitatory population (E) and an inhibitory population (I). These populations interact with each other through feedforward intracortical axodendritic connections, represented by N_{ei} and N_{ie}. The interaction of neurons within each population is represented by feedback intracortical axodendritic connections, represented by N_{ee} and N_{ii}. Extracortical inputs to populations E and I are represented by p_{ee} and p_{ei}, respectively. The topology of the NCM-AHE model is depicted in Fig. 1.

The cortical activity of this model is characterized by the soma membrane potential of each population ($V_k(t), k \in \{e, i\}$), which follows the convolution-based rule and is described by.

$$\tau_k \frac{dV_k(t)}{dt} = V_k^{rest} - V_k(t) + \sum_{l=e,i} \frac{V_l^{eq} - V_k(t)}{\left|V_l^{eq} - V_k^{rest}\right|} I_{lk}(t) \tag{1}$$

where subscripts $k, l \in \{e, i\}$ represent the excitatory population and inhibitory population respectively; V_k^{rest} indicates the resting membrane potential of population k, and V_l^{eq} is the reversal membrane potential of population l; $I_{lk}(t)$ represents the postsynaptic potential (PSP) arriving from population l, which is modeled as the damped oscillation function of incoming axonal pulses:

$$\begin{aligned} DI_{lk}(t) &= \Psi_l A_{lk}(t), \\ D &= \begin{cases} \left(\frac{1}{\gamma_l}\frac{d}{dt} + 1\right)^2, l = e \\ \left(\frac{1}{\gamma_l}\frac{d}{dt} + 1\right)\left(\frac{1}{\tilde{\gamma}_l}\frac{d}{dt} + 1\right), l = i \end{cases}, \\ \Psi_l &= \begin{cases} \frac{e\Gamma_l(t)}{\gamma_l}, l = e \\ \frac{e^{\gamma_l/\gamma_l^0}\Gamma_l(t)}{\gamma_l}, l = i \end{cases}. \end{aligned} \tag{2}$$

Here, D represents a damped oscillator, where γ_l characterizes the exponential decay time scale of the excitatory $(l = e)$ or inhibitory $(l = i)$ PSP, and γ_l^0 is the baseline synaptic time constant. $A_{lk}(t)$represents

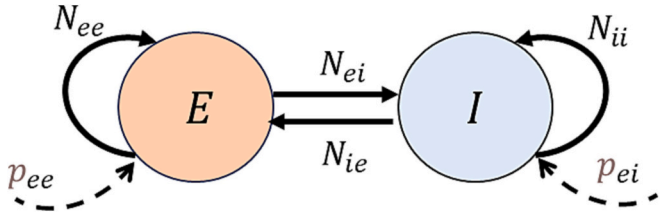

Fig. 1. Schematic of the NCM-AHE model. *E*: excitatory population; *I*: inhibitory population; N_{ei} or N_{ie}: inter-connections from *E* to *I* or from *I* to *E*; N_{ee} or N_{ii}: intra-connections within population *E* or population *I*; p_{ee} or p_{ei}: extracortical inputs to population *E* or population *I*.

the mean rate of incoming pulses from population l, which is assumed to be a sigmoidal function of $V_l(t)$, coupled with an additional extracortical synaptic input $p_{lk}(t)$ (if it exists), given by:

$$A_{lk}(t) = N_{lk}S_l(V_l(t)) + p_{lk}(t),$$
$$S_l(V_l) = \frac{S_l^{max}}{\left(1 + exp\left(-\sqrt{2}\ \frac{(V_l(t) - \mu_l)}{\sigma_l}\right)\right)}, l = e, i. \tag{3}$$

The N_{lk} represents the total number of synaptic connections from population l to population k; $S_l^{max}$is the maximum mean firing rates; μ_l and σ_l are mean and standard deviation values of the firing thresholds in population l, respectively. $\Gamma_l(t)$ is the amplitude of the post-synaptic potential, which satisfies the slow dynamics of itself.

The variable N_{lk} represents the total number of synaptic connections from population l to population k. S_l^{max} is the maximum mean firing rate, while μ_l and σ_l represent the mean and standard deviation values, respectively, of the firing thresholds in population l. $\Gamma_l(t)$ represents the amplitude of the post-synaptic potential, which satisfies its own slow dynamics.

$$\frac{d\Gamma_l(t)}{dt} = \frac{\Gamma_l^{rest} - \Gamma_l(t)}{\tau_l^{rec}} - p_l^{dep}S(V_k(t))\Gamma_k(t),$$
$$\Gamma_l^{rest} = \begin{cases} \Gamma_e^{equ} \times (1 + \mathrm{F}_{am}), l = e \\ \Gamma_i^{rest}, l = i \end{cases}. \tag{4}$$

The variable τ_l^{rec} represents the recovery time for activity-dependent synaptic depression, while p_l^{dep} is the depletion constant reflecting impaired synaptic transmission. Γ_l^{rest} is the resting value of the maximum amplitude of the PSP, and Γ_e^{equ} represents the equilibrium voltage of the excitatory PSP. Finally, F_{am} is the amplification factor.

In summary, the transformations of electrical activities between population l and population k is shown in Fig. 2. In this loop, the membrane potential of population l is first converted into mean firing rate A_{lk} using Eq. (3). Then, it is transformed into post-synaptic potential $I_{lk}(t)$ using Eq. (2). After that the post-synaptic potential $I_{lk}(t)$ inputs into the population k and is transformed into the soma membrane potential V_k according to Eq. (1).

The whole dynamic equations of NCM-AHE are shown as follows (Eq. (5)).

$$\tau_e\frac{dV_e(t)}{dt} = V_e^{rest} - V_e(t) + \frac{V_e^{eq} - V_e}{\left|V_e^{eq} - V_e^{rest}\right|}I_{ee}(t) + \frac{V_i^{eq} - V_e}{\left|V_i^{eq} - V_e^{rest}\right|}I_{ie}(t)$$
$$\tau_i\frac{dV_i(t)}{dt} = V_i^{\mathrm{rest}} - V_i(t) + \frac{V_e^{eq} - V_i}{\left|V_e^{qq} - V_i^{\mathrm{rest}}\right|}I_{ei}(t) + \frac{V_i^{eq} - V_i}{\left|V_i^{eq} - V_i^{\mathrm{rest}}\right|}I_{ii}(t)$$
$$\frac{d^2I_{ee}(t)}{dt^2} + 2\gamma_e\frac{dI_{ee}(t)}{dt} + \gamma_e^2I_{ee}(t) = \Gamma_e(t)\gamma_e e(N_{ee}S_e(V_e, \mu_e) + p_{ee}(t))$$
$$\frac{d^2I_{ei}(t)}{dt^2} + 2\gamma_e\frac{dI_{ei}(t)}{dt} + \gamma_e^2I_{ei}(t) = \Gamma_e(t)\gamma_e e\left(N_{ei}^{\beta}S_e(V_e, \mu_e) + p_{ei}(t)\right),$$
$$\frac{d^2I_{ie}(t)}{dt^2} + (\gamma_i + \widetilde{\gamma}_i)\frac{dI_{ie}(t)}{dt} + \gamma_i\widetilde{\gamma}_iI_{ie}(t) = \widetilde{\gamma}_i\Gamma_i(t)e^{\frac{\gamma_i}{\gamma_i^0}}N_{ie}^{\beta}S_i(V_i, \mu_i),$$
$$\frac{d^2I_{ii}(t)}{dt^2} + (\gamma_i + \widetilde{\gamma}_i)\frac{dI_{ii}(t)}{dt} + \gamma_i\widetilde{\gamma}_iI_{ii}(t) = \widetilde{\gamma}_i\Gamma_i(t)e^{\frac{\gamma_i}{\gamma_i^0}}N_{ii}^{\beta}S_i(V_i, \mu_i). \tag{5}$$

2.2. The computational model of AWD in MHE

To comprehensively understand the role of astrocyte-neuronal communication in the disruption of alpha waves within MHE, our approach involves constructing two fundamental communication pathways. Initially, we establish the feedforward communication pathway originating from the cortical neuron population (CNP) and targeting the astrocyte population (AP). Subsequently, we construct the feedback communication pathway, which operates in the reverse direction from the AP to the CNP. Here, the CNP compartment is constructed using NCM-AHE.

2.2.1. The communication pathway from CNP to AP

We begin by constructing the feedforward communication pathway from the neuron compartment to the astrocyte compartment according to the work (Blanchard et al., 2016), where we describe three state variables: (i) the fluxes of neurotransmitter from neurons to the extracellular space ($J_X, X \in \{Glu, GABA\}$ and Glu represents glutamate while GABA represents gamma-aminobutyric acid), (ii) the concentrations of neurotransmitters in the extracellular space ($[X]_e, X \in \{Glu, GABA\}$), and (iii) the quantity of neurotransmitters recycled and consumed by the astrocytes ($[X]_a, X \in \{Glu, GABA\}$).

The dynamics of J_X are governed by the firing rate $m(t)$ of CNP and transfer function $h_X(t)$, satisfying

$$J_X = m_{e/i}(t) \otimes h_X(t), \tag{6}$$

where $h_X(t)$ is the fundamental solutions for the following differential equations,

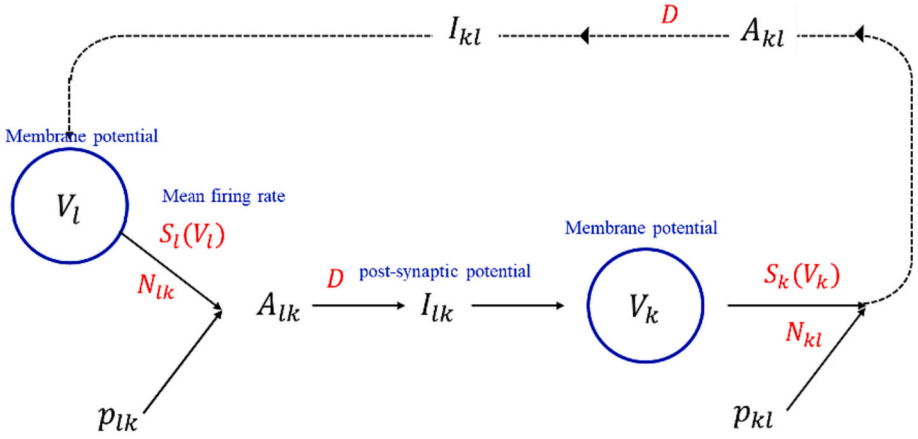

Fig. 2. The paradigm for transformation of electrical activities between population l and population $(k, l \in \{e, i\})$. $A_{lk}(t)$, the mean rate of pulses from population l to k; $I_{lk}(t)$, the postsynaptic potential from population l to k; V_l, soma membrane potential of population l. The V_l is first converted into A_{lk}according to function $S(\cdot)$, which is then transformed into I_{lk} by operator $D(\cdot)$ and inputs into population k to obtain the V_k. Similarly, the dotted line represents the electrical activity transforming from population k to population l in the same manner.

$$F_X(h_X)=\begin{cases}\frac{1}{W}\left(\frac{1}{w_1}\frac{d^2h_{Glu}}{dt^2}+\frac{w_1+w_2}{w_1}\frac{dh_{Glu}}{dt}+w_2h_{Glu}\right), X=Glu\\ \frac{1}{Z}\left(\frac{1}{z_1}\frac{d^2h_{GABA}}{dt^2}+\frac{z_1+z_2}{z_1}\frac{dh_{GABA}}{dt}+z_2h_{GABA}\right), X=GABA\end{cases}.$$

The parameters W and Z are the peak amplitudes of glutamate and GABA; w_1 and w_2 represent the rise and decay times of glutamate transfer function; z_1 and z_2 represent the rise and decay times of GABA transfer function.

Applying Laplace transformation, eq. (6) can be re-expressed as second-order differential equations, as follows:

$$\frac{d^2J_{Glu}}{dt^2}=Ww_1m_e(t)-(w_1+w_2)\frac{dJ_{Glu}}{dt}-w_1w_2J_{Glu},$$

$$\frac{d^2J_{\mathrm{GABA}}}{dt^2}=Zz_1m_i(t)-(z_1+z_2)\frac{dJ_{\mathrm{GABA}}}{dt}-z_1z_2J_{\mathrm{GABA}},$$

$$m_e(t)=S_e(V_e),$$

$$m_i(t)=S_i(V_i).$$

The extracellular glutamate concentration ($[Glu]_e$) is controlled by two pathways: glutamate influx into the extracellular space, and extracellular glutamate uptake by astrocytes and neurons. To model the dynamics of $[Glu]_e$, we rely on the work of (Garnier et al., 2016a), that is,

$$\frac{d[\mathrm{Glu}]_{\mathrm{e}}}{dt}=J_G-\left(V_G^{\mathrm{ae}}+V_G^{\mathrm{ne}}\right)\widehat{\mathscr{S}}\left([\mathrm{Glu}]_{\mathrm{e}},s_g,r_g\right),\tag{7}$$

where $\widehat{S}(\cdot)$ is the uptake function of glutamate by neurons and astrocytes from the extracellular space, satisfying

$$\widehat{S}\left([\mathrm{Glu}]_{\mathrm{e}},s_g,r_g\right)=\frac{1}{\left(1+exp\left(-\sqrt{2}\ \frac{\left([\mathrm{Glu}]_{\mathrm{e}}-s_g\right)}{r_g}\right)\right)}.$$

The V_G^{ae} and V_G^{ne} are the maximum rates of glutamate uptakes by the astrocytes and the neurons; s_g is activation threshold and r_g is the sigmoidal slope of function $\widehat{S}(\cdot)$.

Similarly, the dynamics of extracellular GABA concentrations ($[GABA]_e$) is modeled by

$$\frac{d[\mathrm{GABA}]_{\mathrm{e}}}{dt}=J_{\mathrm{GABA}}-V_\gamma^{\mathrm{ae}}\mathscr{H}\left([\mathrm{GABA}]_{\mathrm{e}},K_\gamma^{\mathrm{ae}}\right)-V_\gamma^{\mathrm{ne}}\mathscr{H}\left([\mathrm{GABA}]_{\mathrm{e}},K_\gamma^{\mathrm{ne}}\right),\tag{8}$$

where $\mathscr{H}(\cdot)$ is the uptake function of GABA by neurons and astrocytes from the extracellular space, satisfying

$$\mathscr{H}(x,k)=\frac{x}{x+k}.$$

In Eq. (8), the first term on the right side represents the fluxes of GABA from the neurons, while the last two terms represent the uptake of GABA by the astrocytes and the neurons, respectively. The parameters V_γ^{ae} and V_γ^{ne} represent the maximum rates of GABA uptake, while K_γ^{ae} and K_γ^{ne} represent the concentrations of GABA transporter for the astrocyte and neuron, respectively.

Lastly, the quantity of neurotransmitters (i.e., Glu and GABA) in the AP is supplied by astrocytic neurotransmitter uptake and is consumed by their degradation. Subsequently, $[\mathrm{Glu}]_{\mathrm{a}}$ and $[\mathrm{GABA}]_{\mathrm{a}}$ can be described using the following equations:

$$\frac{d[\mathrm{Glu}]_{\mathrm{a}}}{dt}=V_G^{\mathrm{ae}}\widehat{\mathscr{S}}\left([\mathrm{Glu}]_{\mathrm{e}},s_g,r_g\right)-V_G^c[\mathrm{Glu}]_{\mathrm{a}},\tag{9}$$

$$\frac{d[\mathrm{GABA}]_{\mathrm{a}}}{dt}=V_\gamma^{\mathrm{ae}}\mathscr{H}\left([\mathrm{GABA}]_{\mathrm{e}},K_\gamma^{\mathrm{ae}}\right)-V_\gamma^c[\mathrm{GABA}]_{\mathrm{a}},\tag{10}$$

where V_G^c and V_γ^c represent the degradation rates of glutamate and GABA in astrocytes respectively (Garnier et al., 2016a).

2.2.2. The communication pathway from AP to CNP

In this part, we will construct the feedback communication pathway from the astrocyte compartment to the neuron compartment.

Previous studies have shown that feedback from the AP onto the CNP could modulate neuron excitability, where extracellular concentrations of neurotransmitters act on the excitability threshold during this process (Araque et al., 1998). Under such recognition, we re-model the firing threshold of the CNP based the extracellular neurotransmitter concentrations following the methodology outlined in (Garnier et al., 2016a) and incorporate it into the conversion process of neural population potentials in NCM-AHE.

In NCM-AHE, the membrane potential of population j $(i.e., V_j, j=e,i)$ is converted into population firing rate $m_j(t)$ by

$$m_j(t)=S_j(V_j)=\frac{S_j^{max}}{\left(1+exp\left(-\sqrt{2}\ \frac{(V_j-\mu_j)}{\sigma_j}\right)\right)},\quad j=e,i.$$

Here, the firing threshold μ_j $(j=e,i)$ is a constant.

To model the impact of extracellular neurotransmitters (glutamate and GABA) on excitability of neural population, the firing thresholds μ_e and μ_i are re-formulated based their concentrations. It is known that the excitability of population E is enhanced by the presence of glutamate in the extracellular space, which can be modeled by a decrease in threshold μ_e. In other words, the concentration of glutamate $\left([\mathrm{Glu}]_{\mathrm{e}}\right)$ is inversely correlated with μ_e. Conversely, GABA inhibits the excitability of E, which can be modeled by an increase in threshold μ_e, thus the concentration of GABA $\left([\mathrm{GABA}]_{\mathrm{e}}\right)$ is positively correlated with μ_e. Gathering both impact of $[\mathrm{Glu}]_{\mathrm{e}}$ and $[\mathrm{GABA}]_{\mathrm{e}}$ on excitability of population E, we set μ_e as

$$\mu_e=\mu_{e0}+m_\gamma\widehat{\mathscr{S}}\left([\mathrm{GABA}]_{\mathrm{e}},v_\gamma,r_\gamma\right)-m_G^P\widehat{\mathscr{S}}\left([\mathrm{Glu}]_{\mathrm{e}},v_G,r_G\right).\tag{11}$$

The parameters μ_{e0} is the basic excitability thresholds for population E; m_G^P is the maximal coupling gain of glutamate feedback on excitatory neurons; m_γ represents the maximal coupling gain of GABA feedback on excitatory neurons.

Glutamate also enhances the excitability of population I, which is modeled by a decrease in threshold μ_i, that is,

$$\mu_i=\mu_{i0}-m_G^I\widehat{\mathscr{S}}\left([\mathrm{Glu}]_{\mathrm{e}},v_G,r_G\right).\tag{12}$$

The parameters μ_{i0} is the basic excitability thresholds for population I and m_G^I is the maximal coupling gain of glutamate feedback on inhibitory neurons.

Based on the population dynamics and transformation of electrical activities in model NCM-AHE, the proposed neural computational model of AWD in MHE (MHE-AWD-NCM) can be formulated by combining the mathematical expressions (6)–(12) of astrocyte-neuronal communication pathways. Fig. 3 shows the sketch of the MHE-AWD-NCM model.

3. Results

3.1. Parameters and simulation

The aim of the study is to examine how disruptions in astrocyte-neuronal communication impact the alpha rhythm, particularly its frequency and power spectra density, in MHE using simulations. To achieve this, the power spectra analysis approach is utilized on simulated EEG signals. These signals are generated through the fourth-order Runge-Kutta method for integrating all differential equations of proposed MHE-AWD-NCM model, and the soma membrane potential of the excitatory

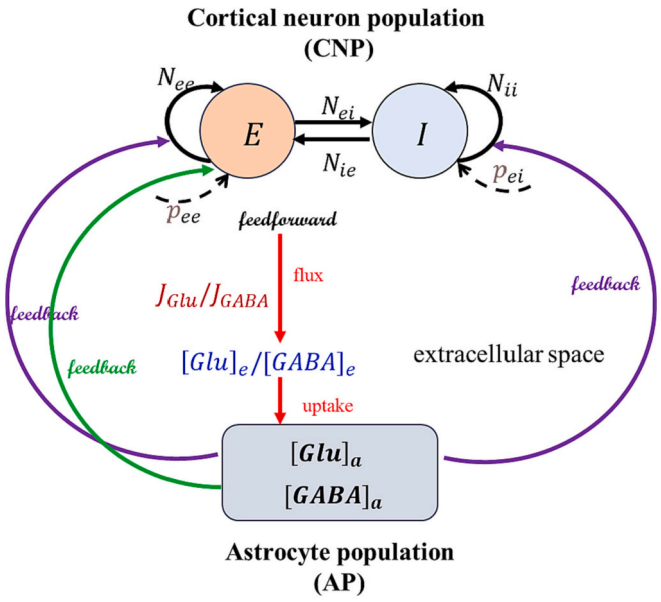

Fig. 3. The sketch of MHE-AWD-NCM model, which is consisted of a cortical neuron population (CNP) and an astrocyte population (AP). The feedforward communication from CNP to AP (shown as the red line with an arrow) is controlled by the fluxes of Glu and GABA (i.e., J_{Glu}/J_{GABA}), as well as their uptake by AP. The feedback communication from AP to CNP is controlled by Glu (i.e., m_G^P and m_G^I) or GABA (i.e., m_γ) feedback gain parameters, where m_G^I only affects population I (shown as the green curve with an arrow); both m_G^P and m_γ affect population E (shown as the purple curve with an arrow).

population (i.e. V_e) is taken to represent the simulated EEG signal. Each simulation has a total simulation time of 30 s at a sampling rate of 250 Hz. The first 20 s of signals are removed, and each simulated signal is then subjected to bandpass filtering using a Butterworth filter of order 10.

For each filtered simulated EEG signal, we calculate the power spectral density within the alpha band (7.5 Hz–13.5 Hz) using a Welch periodogram with a boxcar window of segment length equal to half the sampling frequency and an overlap of 50 %. Subsequently, we define the highest value of power spectral density within the alpha band as the "peak power density," and its corresponding frequency is referred to as the "peak frequency." In the following, we apply peak power density and peak frequency to investigate the effects of astrocyte-neuronal communication, including feedforward and backward communication, on alpha wave disturbance in MHE.

Besides, it is known that MHE patient is often accompanied with cognitive impairments (Guo et al., 2022). A lot of studies have reported a decrease in the power of low-alpha band in individuals with mild cognitive impairments in comparison to healthy individuals (Guo et al., 2022). It sometimes refers to "slowing in the low-alpha frequency range", which is often associated with a decrease in cognitive or mental processing speed. To explore the variation of spectra EEG power within low-alpha band in MHE, we further divide the alpha band into the low-alpha band (7.5-10 Hz) and high-alpha band (10–13.5 Hz), then calculate its spectra power respectively. The simulations and analysis programs were coded in the MATLAB programming language. A noise realization was added at each step to Eq. (10). The nominal values of all parameters in our proposed model are listed in Table 1 (as referenced in (Garnier et al., 2016a; Song et al., 2019)).

3.2. Results

We first demonstrate that our proposed model MHE-AWD-NCM is capable of simulating alpha activity. Fig. 4(a) shows the generated EEG signals with a duration of 20 s, excluding the first 10 s to eliminate any transient effects, while the power spectra density is depicted in Fig. 4(b). It is seen that the power of EEGs is mainly concentrated in alpha band (i.e., 7.5–13.5 Hz). In addition, the mean peak power density and mean peak frequency of 10 trials were also calculated (Fig. 4(c)). In all trails, the model parameters were set to their nominal values.

Table 1
Nominal values of all parameters in MHE-AWD-NCM.

Parameter	Values (units)	Parameter	Values (units)	Parameter	Values (units)
V_e^{rest}, V_i^{rest}	-70 mV	γ_i^0	65/s	m_G^P	2.5 mV
Γ_e^{rest}	0.71 mV	S_e^{max}, S_i^{max}	500/s	m_G^I	1 mV
τ_e, τ_i	94 ms	P_e^{dep}, P_i^{dep}	0.003	m_γ	1 mV
V_e^{eq}	45 mV	W, Z	$53.6\mu M/s$	K_γ^{ae}	$8\mu M$
V_i^{eq}	-90 mV	w_1, z_1	90/s	K_γ^{ne}	$24\ \mu M$
σ	5 mV	w_2, z_2	33/s	μ_{e0}, μ_{i0}	-50 mV
γ_e	300/s	V_G^{ne}	$0.5\mu M/s$	ν_G	$30\mu M$
N_{ee}, N_{ei}	3000	V_G^{ae}	$4.5\ \mu M/s$	r_G	$0.15/\mu M$
N_{ie}, N_{ii}	500	V_γ^{ne}	$5\ \mu M/s$	ν_G	$25\mu M$
V_γ^{ae}	$2\ \mu M/s$	V_G^c, V_γ^c	$9\ \mu M/s$	r_G	$0.12/\mu M$

3.2.1. The effect of feedback communication (AP→CNP) on AWD

The above illustration demonstrates that the feedback communication from the AP to the CNP (including population E and population I) is dependent on the firing threshold parameters μ_e and μ_i. These parameters are modulated by the coupling functions of glutamate and GABA (Eq.(11) and Eq.(12)), which are represented by $m_\gamma \widehat{\mathscr{S}}([\mathrm{GABA}]_e, \nu_\gamma, r_\gamma)$, $m_G^P \widehat{\mathscr{S}}([\mathrm{Glu}]_e, \nu_G, r_G)$ and $m_G^I \widehat{\mathscr{S}}([\mathrm{Glu}]_e, \nu_G, r_G)$ respectively. To explore the role of feedback communication from the AP to the CNP in disturbing alpha waves of MHE, we varied the feedback gain parameters m_G^I, m_G^P,and m_γ of these three coupling functions in our experiments. In the following, we present the AP feedback communication on population I and population E when each is operating in isolation and explore their effects on the disturbance of alpha rhythm in MHE.

3.2.1.1. The AP feedback communication on population I. For population I, it is only affected by glutamate feedback. To investigate the effect of glutamate feedback from AP to population I on AWD, we vary the parameter m_G^I from its normal value of 1 mV to a higher value of 10 mM, while keeping m_G^P and m_γ fixed at their nominal values (i.e., 2.5 mV and 1 mV). The other parameters are also set to be their nominal values, as listed in Table 1. Fig. 5(a) shows the simulated EEG power density curves within the alpha band for five different values of m_G^I, i.e., 1 mV, 3 mV, 5 mV, 7 mV, and 9 mV. The peak power densities for these values are −10.63 dB, −21.97 dB, −23.33 dB, −25.92 dB, and − 26.04 dB, respectively, with corresponding peak frequencies of 11.90, 11.65, 9.83, 8.93, and 9.02 Hz. Approximately, the peak power density and peak frequency of EEGs within alpha band decrease with the increasing values of m_G^I. The overall relationship between m_G^I and peak power density is shown in Fig. 5(b). It can be observed obviously that the peak power density remarkably decreases within the alpha band with the increasing of m_G^I. In addition, the overall relationship between m_G^I and peak frequency is depicted in Fig. 5(c). It also can be seen that increasing m_G^I leads to a clear downward trend in peak frequency. Both the decrease in peak power density and in peak frequency implies that there is a slowing of the alpha band with the increase of m_G^I.

The parameter m_G^I represents strength of glutamate feedback on population I from the AP. A larger value of m_G^I indicates that more excitatory neurotransmitters excite inhibitory neurons, resulting in more intense activity of population I. In turn, the active population I will influence and impose more inhibition on population E, leading to the suppression of activity of excitatory neurons. Therefore, we may hypothesize that increasing glutamate feedback from the AP to CNP may slow down the alpha oscillatory activity. Besides, Fig. 5(d) shows

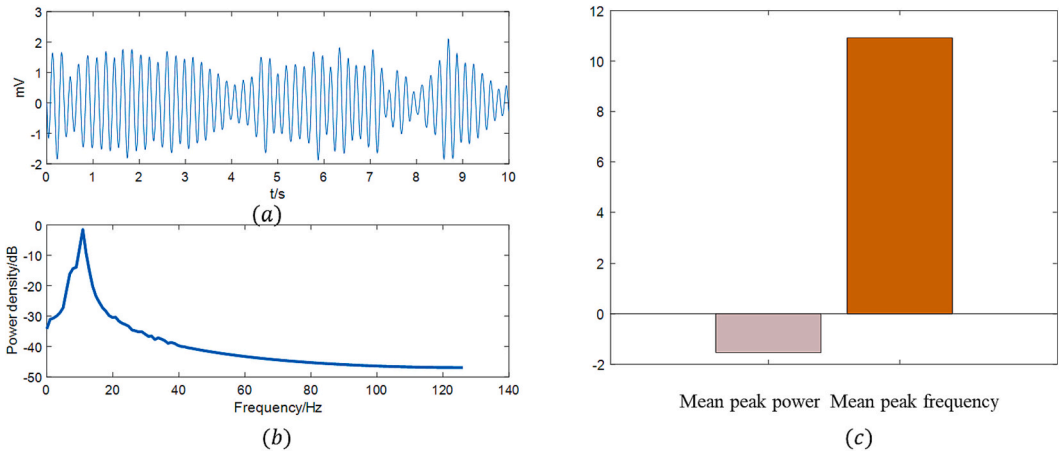

Fig. 4. (a)-(b) The simulated EEG signals with duration of 10 s (a), with the corresponding power spectra density (b); (c) The mean peak power density and mean peak frequency of 10 trials.

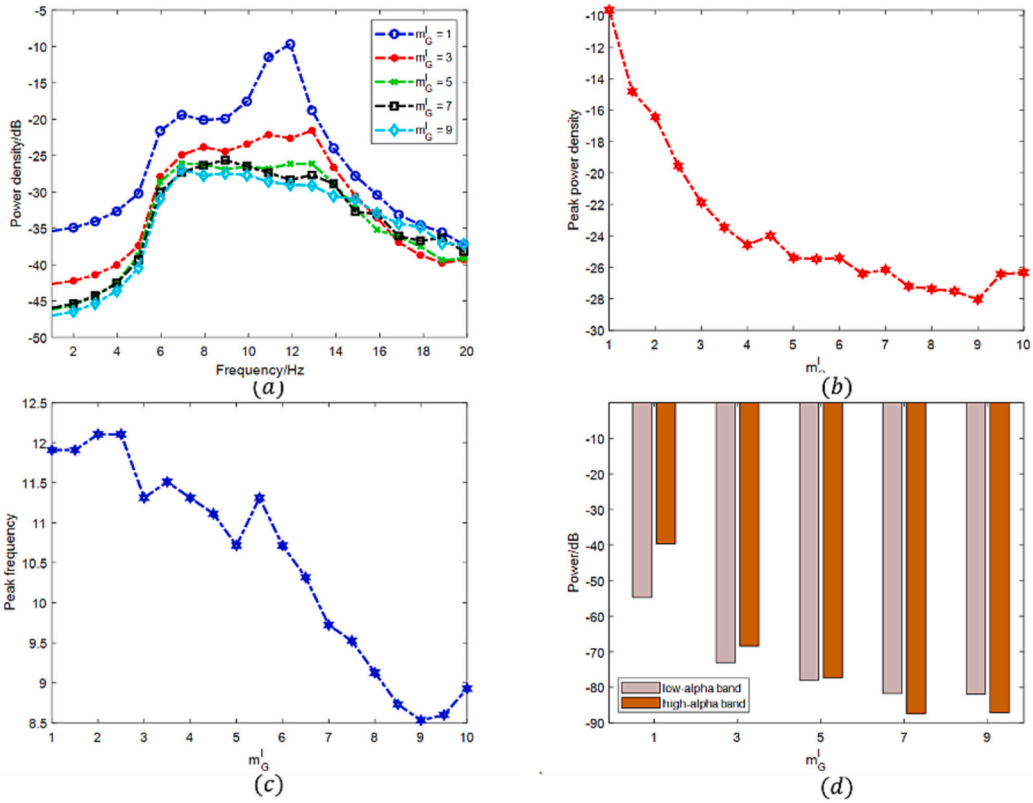

Fig. 5. (a) the simulated EEG power density curves within alpha band for five different values of m_G^I; (b)-(c): the relationship between peak power density and peak frequency of EEGs within alpha band and m_G^I; (d) variations of power in low-alpha and high-alpha bands with m_G^I.

variations of power in low-alpha and high-alpha bands with the increasing m_G^I. We can see that the obvious reduction of power in low alpha band occurred, which is consistent with the findings in physiological research.

3.2.1.2. The AP feedback communication on population E. For population E, it is simultaneously affected by both glutamate feedback and GABA feedback. To investigate the effect of GABA feedback from AP to population E on AWD, we vary the parameter m_γ from its normal value of 1 mV to a higher value of 10 mV. The other parameters are set to their nominal values according to Table 1. Fig. 6(a) shows the five power density curves within alpha band of the simulated EEGs with $m_\gamma = 1,3,5,7,9$mV, where the peak power densities are −17.62 dB, −25.35 dB, −26.21 dB, −27.89 dB, −26.35 dB, and their corresponding peak frequencies are 12.01, 12.95, 9.92, 8.52, and 8.43 Hz, respectively. With the increase of m_γ, there is a trend of reducing the values of peak power density and their corresponding frequencies.

The overall relationships between m_γ and peak power density, as well as peak frequency, are depicted in Figs. 6(b) and 6(c), respectively. It can be observed that both peak power density and peak frequency decrease with increasing coupling gain (i.e., m_γ) of GABA feedback. It is consistent with the fact that the larger the value of m_γ, the greater the inhibition imposed on population E from AP, which further leads to more inactive of population E. We may hypothesize that increasing

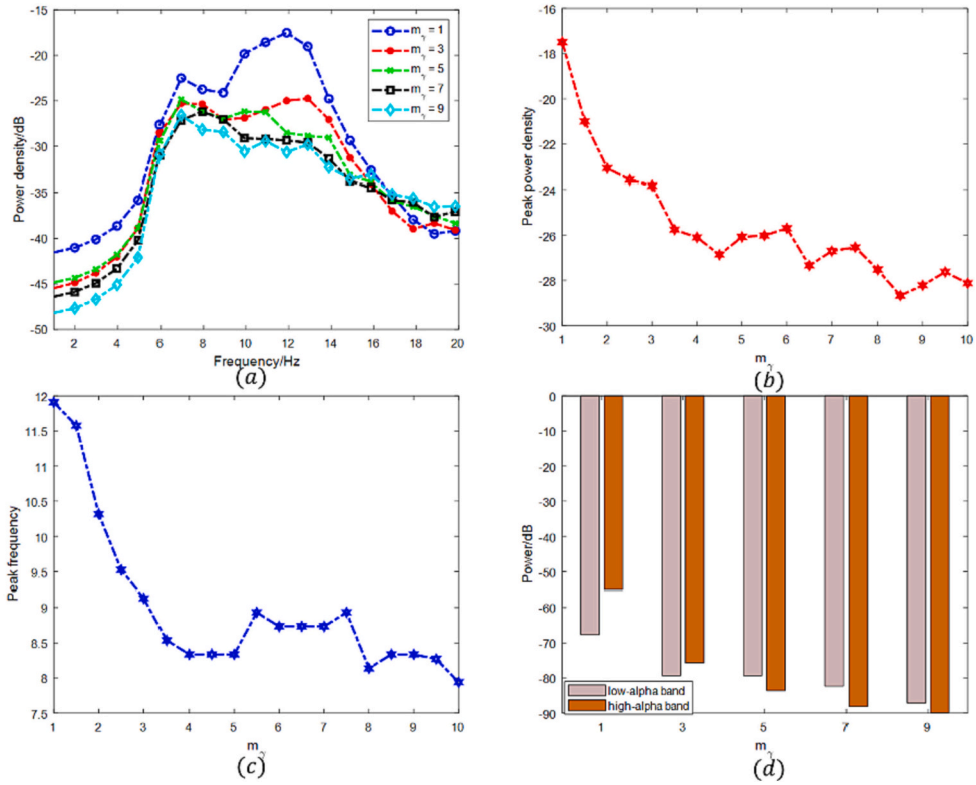

Fig. 6. (a) the simulated EEG power density curves within alpha band for five different values of m_γ; (b)-(c): the relationship between peak power density and peak frequency of EEGs within alpha band and m_γ; (d) variations of power in low-alpha and high-alpha bands with m_γ.

GABA feedback from AP to CNP may disturb or slow down the alpha oscillatory activity (decrease in peak power density and in peak frequency within alpha band). Fig. 6(d) also shows the obvious reduction of power in low-alpha band with the increasing m_γ.

On the other hand, to investigate the effect of glutamate feedback from AP to population E on AWD, the parameter m_G^P is varied from its nominal value of 2.5 mV to a lower value of 0 mV. The other parameters are set according to Table 1. Fig. 7(a) illustrates the power spectral density curves for some typical coupling gain values, that is, $m_G^P = 0.5, 1, 1.5, 2, 2.5$mV. The corresponding peak power densities are 25.65 dB, −23.71 dB, −22.63 dB, −19.93 dB, and − 18.32 dB, and their peak frequencies are 9.79, 12.05, 11.87, 11.73, and 12.92 Hz, respectively.

The overall relationships between m_G^P and peak power density, as well as peak frequency, are shown in Figs. 7(b) and (c). It can be observed that the peak power density has an obvious decreasing trend. The smaller the value of m_G^P, the less excitation will be imposed on E from AP, leading to less active in population E. However, the plot of peak frequency is fairly flat until m_G^P reaches a certain value of about 1.5 mV, after which the peak frequency falls sharply with the decreasing value of m_G^P. Fig. 7(d) also shows the obvious reduction of power in low-alpha band with the decreasing m_γ.

3.2.1.3. The overall effect of AP feedback communication on AWD. Fig. 8 (a) shows the relationship between m_G^P, m_G^I, and peak power density within the alpha band, where $m_G^P \in [0, 2.5]$ with the step of 0.5, and $m_G^I \in [0, 10]$ with the step of 1. It can be observed that as m_G^I increases and m_G^P decreases, the peak power density decreases. Similar results are obtained regarding the relationship among m_G^P, m_G^I, and peak frequency (shown in Fig. 8(d)). That is, decreasing glutamate feedback on population E, and increasing glutamate feedback on population I from the AP will promote the slowing of alpha band. Similarly, the relationship between m_G^P, m_γ, and peak power density, as well as peak frequency are depicted in Fig. 8 (b) and (e) respectively. Both decreasing glutamate feedback and increasing GABA feedback on population E from the AP will promote the slowing of alpha band.

The relationship among m_G^I, m_γ and peak power density is depicted in Fig. 8(c), where both m_G^I and m_γ belongs to $[0, 10]$mV with the step of 1 mV. We can see that peak power density and peak frequency within alpha band decrease with increasing of m_G^I and m_γ. That is, increasing glutamate feedback on population I and GABA feedback on population E from the AP will promote the slowing of alpha band.

3.2.2. The effect of feedforward communication (CNP→AP) on AWD

The illustration above demonstrates that the feedforward communication from CNP to AP is influenced by the release of neurotransmitters from neurons to extracellular space and uptake rates of neurotransmitters by the astrocytes.

3.2.2.1. The neurotransmitter release from CNP to the extracellular space. To investigate the impact of glutamate and GABA fluxes from the CNP to the extracellular space on AWD in MHE, we manipulated key model parameters that represent the peak amplitude of glutamate and GABA concentration (referred to as W and Z, respectively) in our experiments.

Glutamate release from CNP (varying of W*).* We increase the value of W from its normal level of $53.6 \times 10^{-6} mM/ms$ to higher level $53.6 \times 10^{-1} mM/ms$ in our experiments. Specifically, we set W to be $53.6{*}10^{-j}\ mM/ms$, $(j \in \{2, 3, 4, 5, 6\})$. Fig. 9(a) displays the corresponding power spectral densities for these five values of W. It can be observed that as W increases, the peak power density also increases while the peak frequency decreases. The stronger positive correlation between W and peak power density, as well as negative correlation between W and peak frequency, are illustrated in Fig. 9(b) and Fig. 9(c). Furthermore, Fig. 9(d) demonstrates a noticeable reduction in power within both the low and high-alpha bands as W decreases.

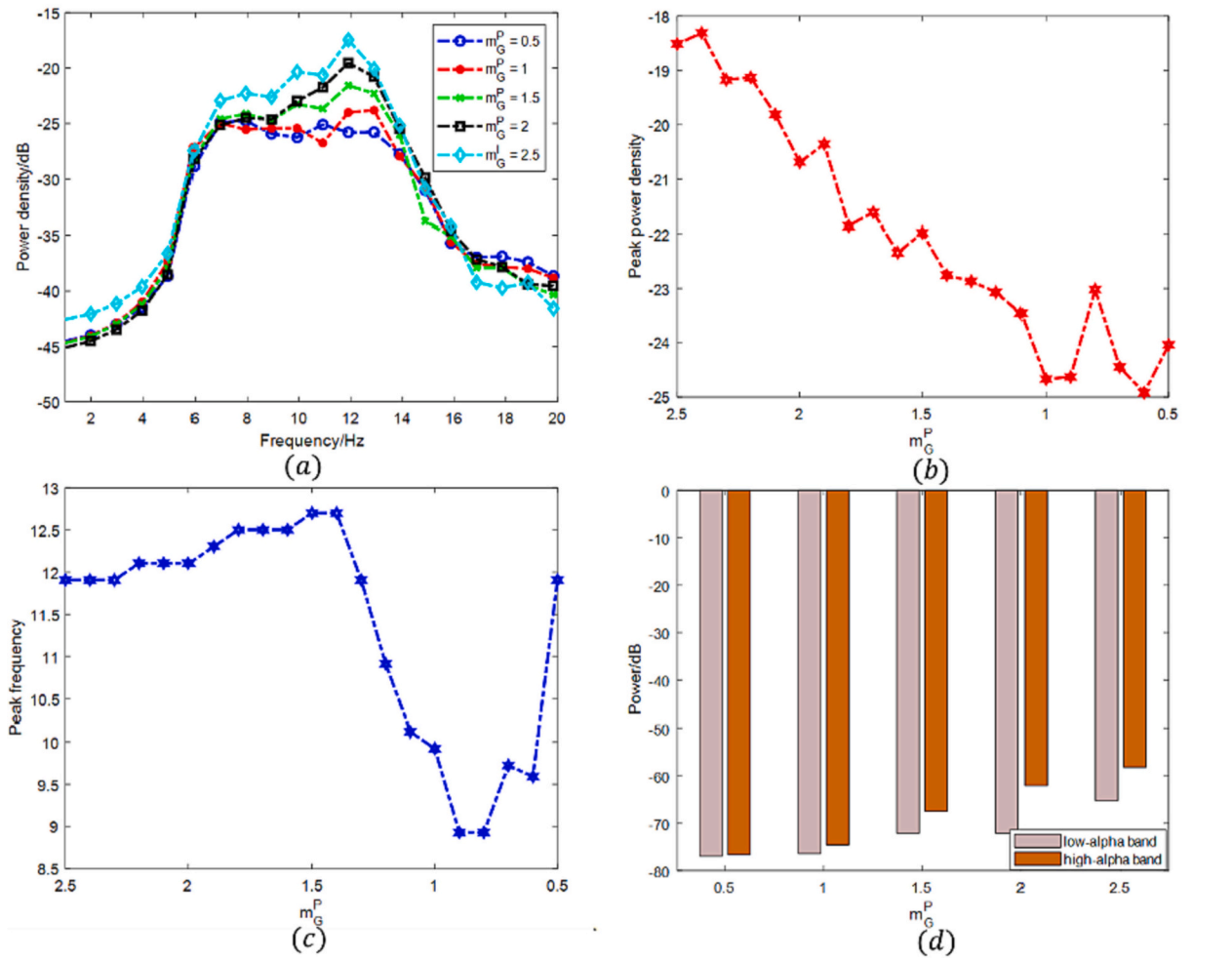

Fig. 7. (a) the simulated EEG power density curves within alpha band for five different values of m_G^P; (b)-(c): the relationship between peak power density and peak frequency of EEGs within alpha band and m_G^P; (d) variations of power in low-alpha and high-alpha bands with m_G^P.

GABA release from CNP (Varying of Z). In our experiments, we increase Z from its normal value of $53.6 \times 10^{-6} mM/ms$ to higher value $53.6 \times 10^{-1} mM/ms$. Specifically, it is set to be $53.6*10^{-j}\ mM/ms$, $(j \in \{2,3,4,5,6\})$. Fig. 9(e) shows the corresponding power spectral densities for these values of Z. We can see that both peak power density and peak frequency decrease with the increasing of Z. The stronger negative correlation between Z and peak power density, as well as peak frequency are depicted in Fig. 9(f) and Fig. 9(g). We may hypothesize that increasing GABA flux from CNP to extracellular space may disturb or slow down the alpha oscillatory activity. Fig. 9(h) shows the obvious reduction of power in both low and high-alpha bands with the increasing Z.

3.2.2.2. The uptake of neurotransmitters by the AP. To explore the role of astrocytic glutamate and GABA uptake in AWD of MHE, we varied key model parameters representing the uptake rates of glutamate and GABA by the AP (i.e., V_G^{ae}, V_γ^{ae}) in our experiments.

Glutamate uptake by the AP (Varying of V_G^{ae}). We decrease V_G^{ae} from value of $4.5 \times 10^{-5} mM/ms$ to lower value $4.5 \times 10^{-9} mM/ms$ in our experiments (the nominal value is $4.5 \times 10^{-6} mM/ms$). Specifically, we set V_G^{ae} to be $4.5*10^{-j}\ mM/ms$, $(j \in \{5,6,7,8,9\})$, respectively. The five curves in Fig. 10(a) are corresponding power spectra densities, where we can see that the peak power density with alpha band increases with the decrease of V_G^{ae}. The negative correlations between V_G^{ae} and peak power density is depicted in Fig. 10(b). However, the positive correlations between V_G^{ae} and peak frequency is depicted in Fig. 10(c), where the peak frequency decreases with the decreased V_G^{ae}.

The decrease in V_G^{ae} implies a reduction of astrocytic glutamate uptake, resulting in a higher glutamate concentration in the extracellular space. This effect is similar to the increase in W. From Fig. 10 (c) (or Fig. 9 (c)), we can observe that peak frequency within alpha bands is decreasing, the hallmark of MHE-EEG, with the decrease of V_G^{ae} (or increase of W). This is consistent with that in physiological experiments. In the study by (Rose, 2002), it was highlighted that the elevation of extracellular brain glutamate in the development of HE is primarily attributed to the hindrance of glutamate uptake by astrocytes. Furthermore, Malaguarnera et al. emphasized that the elevated levels of glutamate in the extracellular fluid of the brain are believed to contribute to the pathogenesis of MHE. However, under such situations (the decrease of V_G^{ae} or increase of W), the decreasing peak power density within alpha band is not occurrence.

GABA uptake by the AP (Varying of V_γ^{ae}). The V_γ^{ae} is decreased from value $2 \times 10^{-5} mM/ms$ to lower value $2 \times 10^{-9} mM/ms$. In specific, we set V_γ^{ae} to be $2 \times 10^{-j} mM/ms, (j \in \{5,6,7,8,9\})$ respectively. The experimental results are shown in Fig. 10(e), where the five curves represent corresponding power spectral densities. Both positive correlation between V_γ^{ae} and peak power density, as well as peak frequency becomes more apparent in Fig. 10(f) and Fig. 10(g). The decrease in peak power density and peak frequency within the alpha band indicates a slowing of the alpha band upon decreasing V_γ^{ae}. Fig. 10(h) shows the

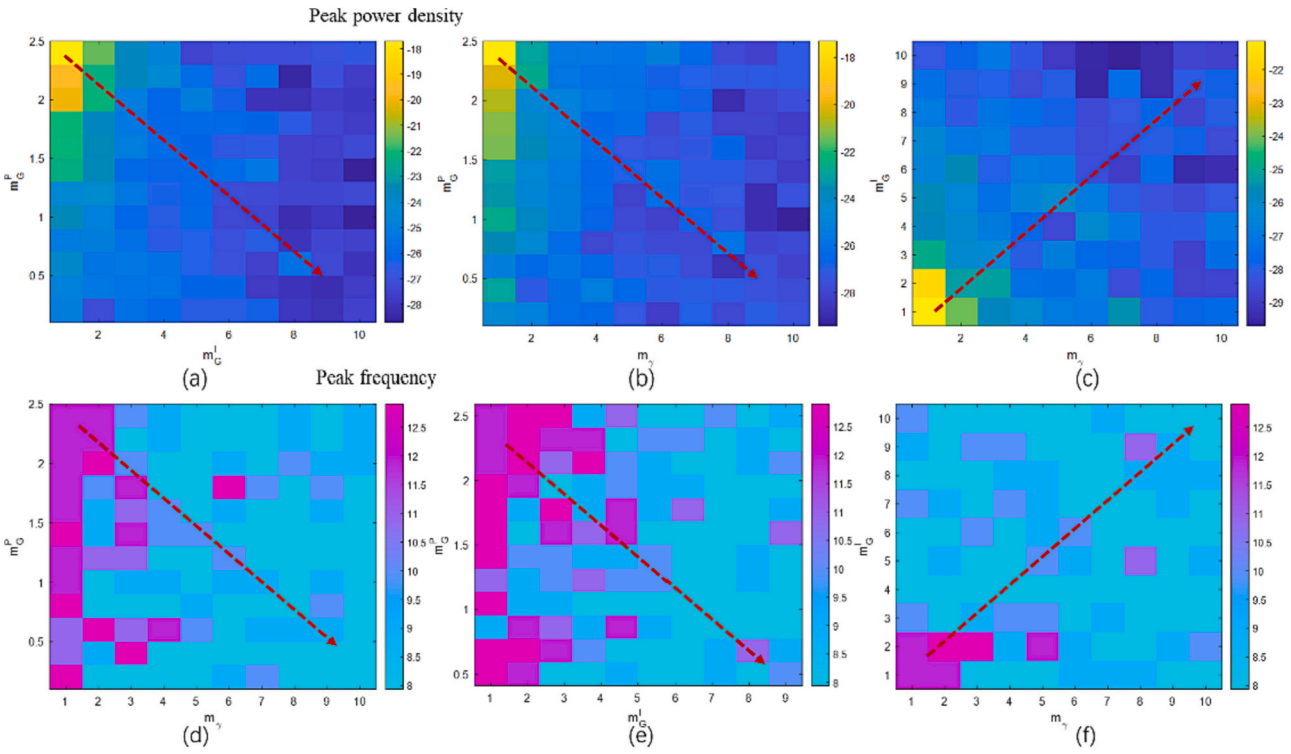

Fig. 8. (a)-(c): The overall effect of AP feedback communication on peak power density within the alpha band. The color bar indicates the value of the peak power density (dB). (d) –(f): The overall effect of AP feedback communication on peak frequency within the alpha band. The corresponding color bar indicates the value of the peak frequency (Hz). (a) and (d): the relationship between m_G^P, m_G^I, and peak power density, as well as peak frequency; (b) and (e): the relationship between m_G^P, m_γ, and peak power density, as well as peak frequency; (c) and (f): the relationship between m_G^I, m_γ, and peak power density, as well as peak frequency. The arrows in each subfigure indicate the overall variation trend for peak power density or peak frequency with the variation of parameter settings.

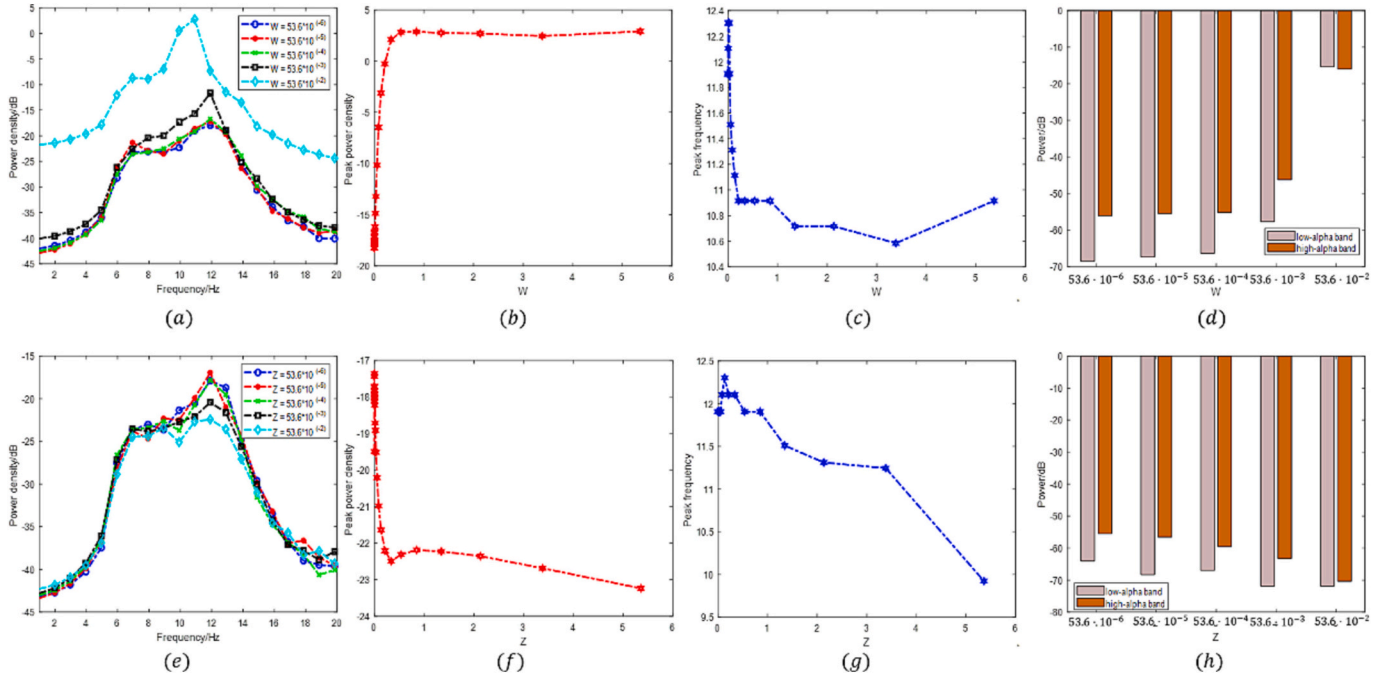

Fig. 9. (a) and (e): the simulated EEG power density curves within alpha band for five different values of W and Z respectively; (b) (or (f)): the relationship between peak power density of EEGs within alpha band and W(or Z); (c) (or (g)): the relationship between peak frequency of EEGs within alpha band and W(or Z); (d) and (h): variations of power in low-alpha and high-alpha bands with W and Z respectively.

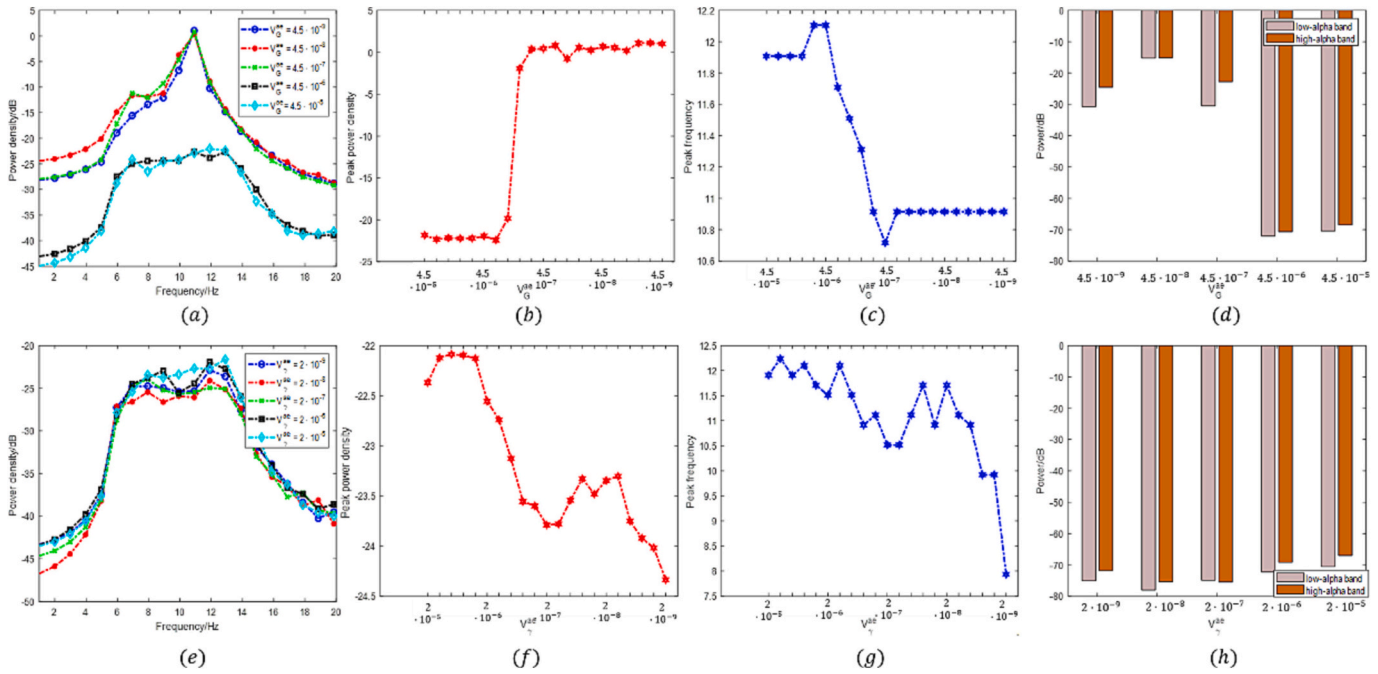

Fig. 10. (a) and (e): the simulated EEG power density curves within alpha band for five different values of V_G^{ae} and V_γ^{ae} respectively; (b) (or (f)): the relationship between peak power density of EEGs within alpha band and V_G^{ae} (or V_γ^{ae}); (c) (or (g)): the relationship between peak frequency of EEGs within alpha band and V_G^{ae}(or V_γ^{ae}); (d) and (h): variations of power in low-alpha and high-alpha bands with V_G^{ae} and V_γ^{ae} respectively.

reduction of power in both low and high-alpha bands with the decreasing V_γ^{ae}.

The reduction in V_γ^{ae} implies a decrease in astrocytic uptake of GABA, leading to an elevated concentration of GABA in the extracellular space. This effect is similar to the increase of parameter Z. From the aforementioned experiments, it is evident that both the peak power density and peak frequency within the alpha bands are decreasing. These alterations align with the usual features of MHE-EEG and are correlated with the decrease in V_γ^{ae}. This consistency is in line with findings from physiological experiments. The recent reports support that neuroinflammation is closely related to altered GABAergic neurotransmission and increased GAT-3 membrane expression and extracellular GABA in MHE (Dadsetan et al., 2016b). Possible mechanisms for this include direct action of ammonia on GABA receptors and inhibition of astrocyte

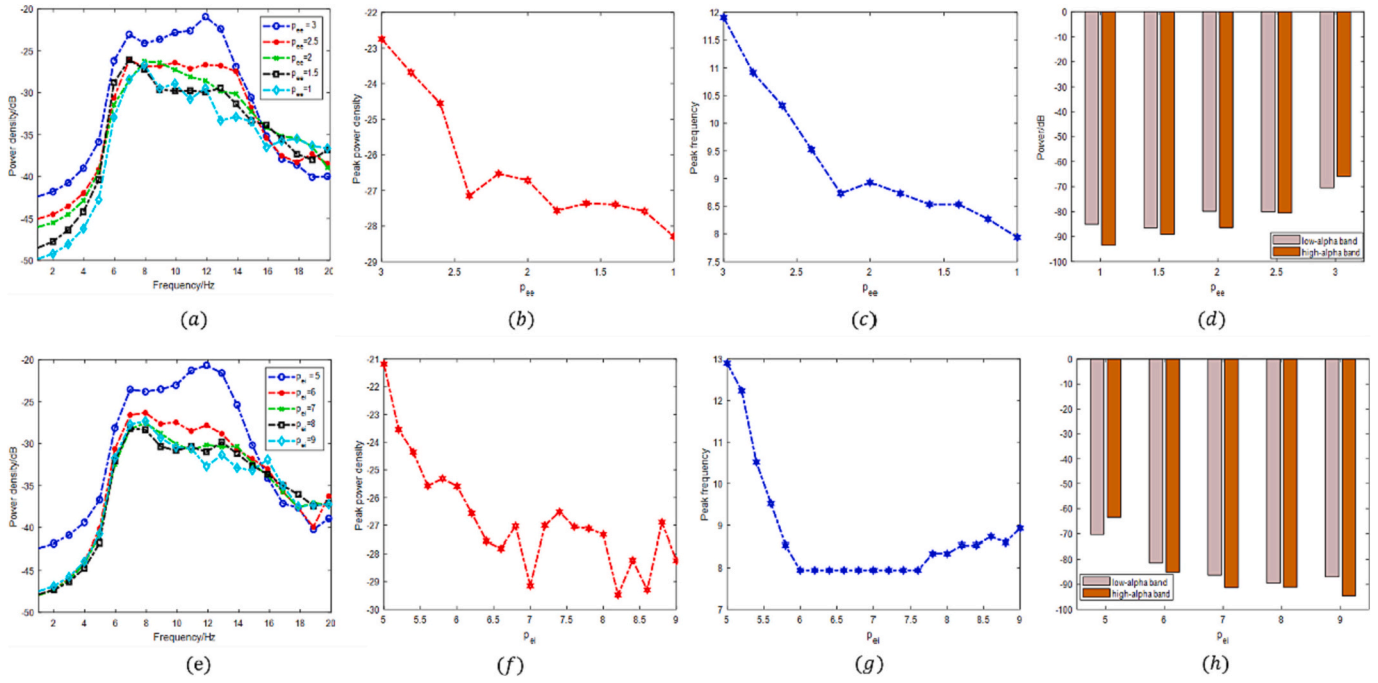

Fig. 11. (a) and (e): the simulated EEG power density curves within alpha band for five different values of p_{ee} and p_{ei},respectively; (b) and (f): the relationship between peak power density within alpha band and p_{ee}, as well as p_{ei}; (c) and (g): the relationship between peak frequency within alpha band and p_{ee}, as well as p_{ei}; (d) and (h): variations of power in low-alpha and high-alpha bands with p_{ee} and p_{ei}.

uptake of GABA thereby resulting in increased levels of extracellular GABA. We may hypothesize that decreasing astrocytic uptake of GABA may disturb or slow down the alpha oscillatory activity.

3.2.3. The effect of external stimulus on AWD

In addition, we try to investigate the effect of external excitatory stimulus for CNP on slowing of alpha showing, where the two model parameters p_{ee} and p_{ei} are varied. The p_{ee} represents the external stimulus on population E, where it decreases from its normal value of 3 to lower value 1 with the step of 0.5 and the corresponding power spectra densities are calculated, as shown in Fig. 11 (a). It can be observed that the peak power densities of EEG signals within alpha band decrease with the decreasing of p_{ee}. The more obvious positive correlations between p_{ee} and peak power, as well as peak frequency are depicted in Figs.11(b) and 11(c). Fig. 11(d) presents the power in low and high-alpha bands, which decreases with the decreasing p_{ee}.

The p_{ei} represents the external stimulus on population I, where it increases from its normal value of 5 to higher value 9 with the step of 1 and the corresponding power spectra densities are calculated, as shown in Fig. 11 (e). It can be observed that the peak power densities of EEG signals within alpha band decrease with the increasing of p_{ei}. The more obvious negative correlations between p_{ei} and peak power, as well as peak frequency are depicted in Figs.11(f) and 11(g). Fig. 11(h) demonstrates that the decreasing power in low-alpha and high-alpha bands with the increase of p_{ei}. These results may indicate that decreased excitatory external stimulus on population E and increased stimulus on population I may promote the slowing of alpha rhythm.

3.3. The sensitivity analysis of key model parameters

The effects of above nine parameters (i.e., m_G^P, m_γ, m_G^I, V_G^{ae}, W, Z, V_G^{ae}, V_γ^{ae},p_{ee},p_{ei}) on peak power density and peak frequency within alpha band in MHE is summarized in Table 2. The upper right '*' and '#' of each parameter represents the increase or decrease of parameter value from its normal value. Increase or decrease in peak power density or peak frequency is shown with a '⇑' or '⇓' respectively, while 'X' implies no definite trend. We can see that the variation of parameters m_γ, m_G^I, Z, V_γ^{ae}, p_{ee}, p_{ei} may induce decrease of both peak power density and peak frequency within alpha band for MHE.

From above illustration, the six parameters m_γ, m_G^I, Z, V_γ^{ae}, p_{ee}, p_{ei} have an impact on the decrease of peak power density and peak frequency within alpha band in MHE. In the following, we analyze sensitivity of above six model parameters using the Morris screening method (Saltelli et al., 2004), to investigate the significance of different parameters on decreasing of peak power density and peak frequency within alpha band. The elementary effect of each parameter θ_i is computed as follows,

$$EE_{i,F}^{j} = \frac{F(\theta_1, \ldots, \theta_i, \ldots, \theta_6) - F(\theta_1, \ldots, \theta_i + \Delta_i, \ldots, \theta_6)}{\Delta_i},$$

$i = 1, 2, \ldots, 6; j = 1, 2, \ldots, r.$

The parameter $\theta_i \in \{m_\gamma, m_G^I, Z, V_\gamma^{ae}, p_{ee}, p_{ei}\}$, which are sampled within their reasonable ranges, and Δ_i is the perturbation of θ_i. The One-At-the-Time sampling strategy with the Latin hypercube method is applied, as described in (Iman, 2008). Here, the $F(\cdot)$ represent the peak power density (PPD) or peak frequency (PF) of simulated EEGs under different parameter values. This process is repeated r times. In our experiments, $r = 50$. Then, 50 values of $EE_{i,F}$ for each θ_i are calculated. Fig. 12 (a) and (b) show the frequency histogram of EE_i $(i = 1, 2, \ldots, 6)$ for peak power density (i.e., $EE_{i,PPD}$) and corresponding "mean-standard deviation" plot of $EE_{i,PPD}$.Fig. 12 (c) and (d) are the frequency histogram of EE_i $(i = 1, 2, \ldots, 6)$ for peak frequency (i.e., $EE_{i,PF}$) and corresponding "mean-standard deviation" plot of $EE_{i,PF}$.

4. Discussions and conclusions

In this study, we introduced a new neural computational model to explore the mechanistic details of alpha wave disturbance (i.e., decreasing of peak power density and peak frequency within alpha band) in MHE. Our model is based on the NCM-AHE, augmented with mathematically characterized mechanisms related to astrocyte-neuronal communication, which plays an important role in disturbance of alpha waves in MHE. The key parameters corresponding to feedforward communication from cortical neuron population (CNP) to astrocyte population (AP) and the feedback communication from AP to CNP are studied to explore how disruption of astrocyte-neuronal communication affects the alpha wave disturbance in MHE. We also conduct the sensitivity analysis of the model to investigate the significance of key model parameters on alpha wave disturbance.

Based on our experiments, it's evident that several parameters, namely m_γ (which represents the strength of GABA feedback on population E from AP), m_G^I (representing the strength of glutamate feedback on population I from AP), Z(indicating the peak amplitude of GABA concentration from CNP to extracellular space), V_γ^{ae} (representing the uptake rates of GABA by the AP), p_{ee}, and p_{ei} (denoting the external excitatory stimulus on populations E and I respectively), have the potential to induce a decrease in both the peak power density and peak frequency within the alpha band, which are characteristics of MHE.

Our experimental findings clearly demonstrate that an increase in glutamate release from the AP onto the inhibitory neuron population, coupled with a decrease in GABA release from the AP onto the excitatory neuron population, is linked to a more pronounced slowing of the alpha band. Besides, a decrease in glutamate release and an increase in GABA

Table 2
A summary of the effects of key parameters on AWD within alpha band in MHE.

	Parameters	Interpretation	Peak power density within alpha band	Peak frequency within alpha band
AP→ CNP	$m_G^{I\,(*)}$	Strength of glutamate feedback on population I	⇓	⇓
	$m_G^{P\,(\#)}$	Strength of glutamate feedback on population E	⇓	X
	$m_\gamma{}^{(*)}$	Strength of GABA feedback on population E	⇓	⇓
	$V_G^{ae\,(\#)}$	Uptake rates of glutamate by the AP	⇑	⇓
CNP→ AP	$V_\gamma^{ae\,(\#)}$	Uptake rates of GABA by the AP	⇓	⇓
	$W^{(\#)}$	Peak amplitude of glutamate concentration	⇑	⇓
	$Z^{(\#)}$	Peak amplitude of GABA concentration	⇓	⇓
External stimulus	$p_{ee}{}^{(\#)}$	External excitatory stimulus on population E	⇓	⇓
	$p_{ei}{}^{(*)}$	External excitatory stimulus on population I	⇓	⇓

(*): the parameter value is increased from its normal value.
(#):the parameter value is decreased from its normal value.
(⇓) decreasing trend; (⇑): increasing trend; (X): no significant decreasing or increasing trend.

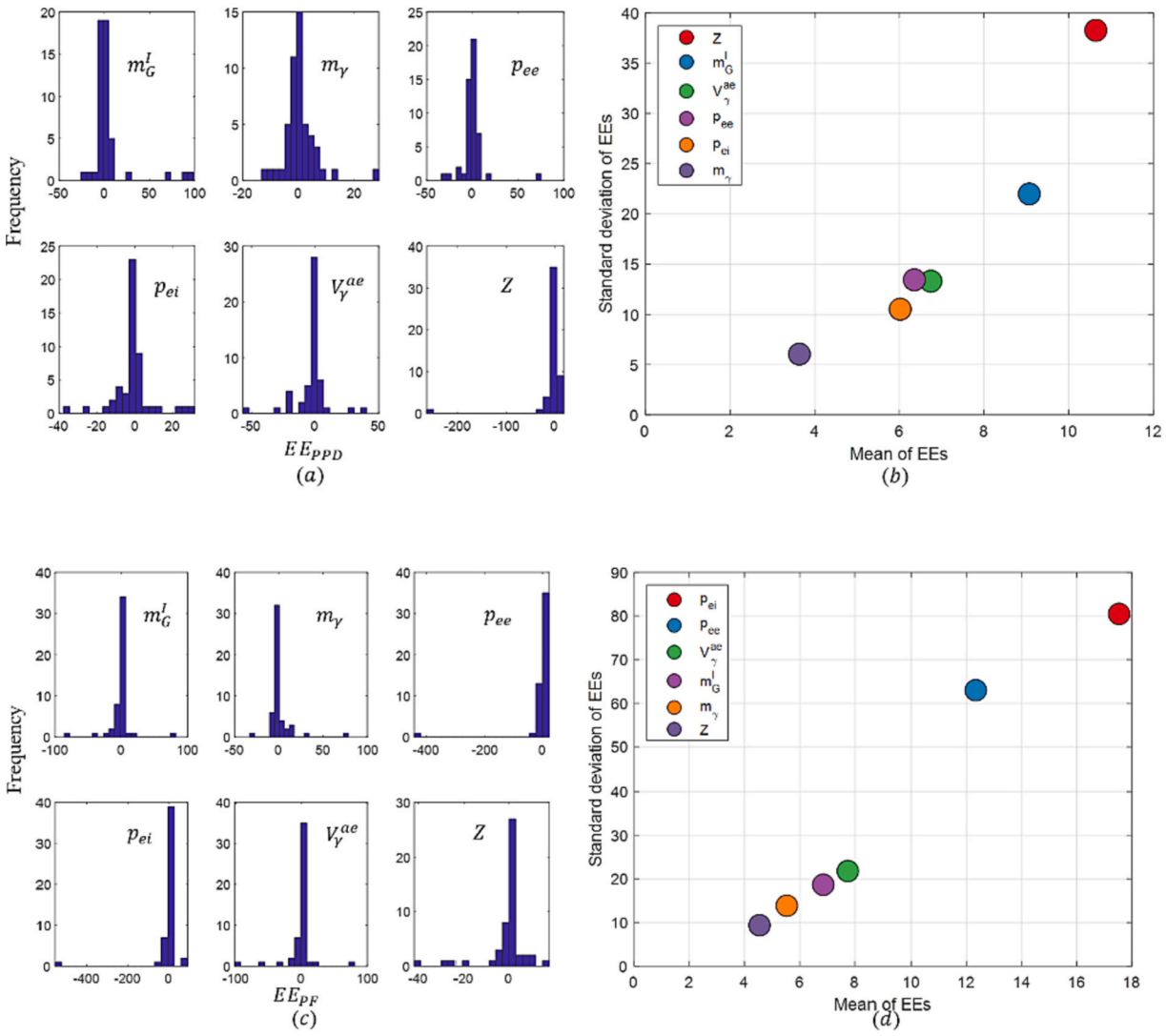

Fig. 12. (a) and (c): The frequency histogram of $EE_{i,F}$ for θ_i, where F represents peak power density (PPD) and peak frequency (PF) respectively; (b) and (d): The "mean-standard deviation" plot of EE_F ($F \in \{PPD, PF\}$)for each θ_i.

release from the AP onto the excitatory neuron population also contribute to the slowing of the alpha band. This slowing serves as a biomarker for MHE. In the work of (Dhiman and Chawla, 2009b), it is highlighted that HE is linked to changes in the expression of genes within astrocytes and neurons. These genes code for different proteins crucial for central nervous system function, encompassing functions such as cell volume regulation and neurotransmission. We can thus speculate that disturbances in neurotransmission from astrocytes to neurons are strongly correlated with the disruption of alpha waves in cases of MHE.

The mounting body of evidence underscores the pivotal role of ammonia in the development of MHE (Dhiman and Chawla, 2009a; Dhiman et al., 2010; Dadsetan et al., 2016a). Ammonia exerts damaging effects on brain metabolism and neurotransmission (Dhiman et al., 2010). Bender et al. demonstrated that ammonia, even at concentrations (5 mM) relevant to hepatic encephalopathy (HE), acutely hindered astrocytic GABA uptake by around 30 %, and after a 4-day treatment, this inhibition increased to 50–60 %. In our study, our experimental results vividly display that reduced uptake rates of GABA by astrocytes, leading to an augmentation of extracellular GABA concentrations, results in a decline of both peak power density and peak frequency within the alpha band. Hence, we can speculate that the gradual accumulation of ammonia in the initial stages of HE inhibits the uptake of GABA by astrocytes. This inhibition could potentially trigger disruptions in alpha waves seen in MHE.

There exists evidence that points to disruptions in the glutamatergic system in MHE, including an elevation in cortical release of glutamate (Glu) and a reduction in Glu uptake by astrocytes and neurons. This imbalance leads to elevated Glu levels in the extracellular fluid of the brain and is proposed to be involved in the development of MHE (Malaguarnera et al., 2018). Additionally, studies by Bender and Norenberg revealed that subjecting primary cultures of astrocytes to ammonia resulted in a significant reduction in the high-affinity uptake of glutamate (Lemberg and Fernández, 2009). Our model further indicates that decreased uptake rates of glutamate by astrocytes contribute to the decline in peak frequency within the alpha band. This frequency alteration serves as a distinctive marker for MHE.

From a different perspective, our findings align with the conclusions of a review study (Butz et al., 2013), which proposes a potential interplay between changes in neurotransmission and oscillatory brain activity in HE. Moreover, it's worth noting that external stimuli also play a role in influencing the disturbance of alpha waves in MHE. Decreasing the excitatory external stimulus on population E and increasing the stimulus on population I contribute to the deceleration of the alpha rhythm. In summary, our research contributes to a deeper comprehension of the neural mechanisms that underlie the slowing of alpha bands

in MHE. This understanding opens up possibilities for prospective therapeutic interventions in the future.

CRediT authorship contribution statement

Jiangling Song: Writing – original draft, Software, Methodology, Investigation, Funding acquisition, Formal analysis. **M. Brandon Westover:** Writing – review & editing, Supervision, Funding acquisition, Conceptualization. **Rui Zhang:** Writing – review & editing, Supervision, Funding acquisition, Conceptualization.

Declaration of competing interest

We declare that we do not have any commercial or associative interest that represents a conflict of interest in connection with the work submitted.

Data availability

No data was used for the research described in the article.

Acknowledgement

Drs. Jiang-Ling Song and Rui Zhang were supported by the National Natural Science Foundation of China under Grants 62006189 and 12071369. Dr. Westover is supported by the Glenn Foundation for Medical Research and the American Federation for Aging Research through a Breakthroughs in Gerontology Grant; through the American Academy of Sleep Medicine through an AASM Foundation Strategic Research Award; and by grants from the NIH (1R01NS102190, 1R01NS102574, 1R01NS107291, 1RF1AG064312).

References

Amodio, P., Montagnese, S., 2015. Clinical neurophysiology of hepatic encephalopathy [J]. J. Clin. Exp. Hepatol. 5, S60–S68.
Araque, A., Parpura, V., Sanzgiri, R.P., Haydon, P.G., 1998. Glutamate-dependent astrocyte modulation of synaptic transmission between cultured hippocampal neurons. Eur. J. Neurosci. 10 (6), 2129–2142.
Bhattacharya, B.S., Coyle, D., Maguire, L.P., 2011. Alpha and Theta Rhythm Abnormality in Alzheimer's Disease: A Study Using a Computational Model[J]. Springer, New York.
Blanchard, S., Saillet, S., Ivanov, A., et al., 2016. A new computational model for neuro-glio-vascular coupling: astrocyte activation can explain cerebral blood flow nonlinear response to interictal events[J]. PLoS One 11 (2), e0147292.
Bojak, I., Stoyanov, Z.V., Liley, D.T.J., 2015. Emergence of spatially heterogeneous burst suppression in a neural field model of electrocortical activity[J]. Front. Syst. Neurosci. 9, 18.
Butz, M., May, E.S., Häussinger, D., et al., 2013. The slowed brain: cortical oscillatory activity in hepatic encephalopathy[J]. Arch. Biochem. Biophys. 536 (2), 197–203.
Ciećko-Michalska, I., Szczepanek, M., Słowik, A., et al., 2012. Pathogenesis of hepatic encephalopathy[J]. Gastroenterol. Res. Pract. 2012.
Dadsetan, S., Balzano, T., Forteza, J., et al., 2016a. Infliximab reduces peripheral inflammation, neuroinflammation, and extracellular GABA in the cerebellum and improves learning and motor coordination in rats with hepatic encephalopathy[J]. J. Neuroinflammation 13 (1), 1–14.
Dadsetan, S., Balzano, T., Forteza, J., et al., 2016b. Infliximab reduces peripheral inflammation, neuroinflammation, and extracellular GABA in the cerebellum and improves learning and motor coordination in rats with hepatic encephalopathy[J]. J. Neuroinflammation 13 (1), 1–14.
Dhiman, R.K., Chawla, Y.K., 2009a. Minimal hepatic encephalopathy[J]. Indian J. Gastroenterol. 28, 5–16.
Dhiman, R.K., Chawla, Y.K., 2009b. Minimal hepatic encephalopathy[J]. Indian J. Gastroenterol. 28, 5–16.
Dhiman, R.K., Saraswat, V.A., Sharma, B.K., et al., 2010. Minimal hepatic encephalopathy: consensus statement of a working party of the Indian National Association for study of the liver[J]. J. Gastroenterol. Hepatol. 25 (6), 1029–1041.
Garnier, A., Vidal, A., Benali, H., 2016a. A theoretical study on the role of astrocytic activity in neuronal hyperexcitability by a novel neuron-glia mass model[J]. J. Math. Neurosci. 6, 1–30.
Garnier, A., Vidal, A., Benali, H., 2016b. A theoretical study on the role of astrocytic activity in neuronal hyperexcitability by a novel neuron-glia mass model[J]. J. Math. Neurosci. 6, 1–30.
Guo, J.R., Shi, J.Y., Dong, Q.Y., et al., 2022. Altered dynamic spontaneous neural activity in minimal hepatic encephalopathy[J]. Front. Neurol. 13, 963551.
Han, W., Zhang, H., Han, Y., et al., 2020. Cognition-tracking-based strategies for diagnosis and treatment of minimal hepatic encephalopathy[J]. Metab. Brain Dis. 35, 869–881.
Hartoyo, A., Cadusch, P.J., Liley, D.T.J., et al., 2020. Inferring a simple mechanism for alpha-blocking by fitting a neural population model to EEG spectra[J]. PLoS Comput. Biol. 16 (4), e1007662.
Häussinger, D., Görg, B., 2019. Oxidative-nitrosative stress andhepatic encephalopathy. In: Sies, H. (Ed.), Oxidative stress: eustress and distress. Elsevier, Cambridge, pp. 669–686.
Häussinger, D., Butz, M., Schnitzler, A., et al., 2021. Pathomechanisms in hepatic encephalopathy[J]. Biol. Chem. 402 (9), 1087–1102.
Iman, R.L., 2008. L atin hypercube sampling[J]. Encyclopedia of quantitative risk analysis and assessment 3.
Lemberg, A., Fernández, M.A., 2009. Hepatic encephalopathy, ammonia, glutamate, glutamine and oxidative stress[J]. Ann. Hepatol. 8 (2), 95–102.
Li, X.Y., Yang, X.L., Sun, Z.K., 2020. Alpha rhythm slowing in a modified thalamo-cortico-thalamic model related with Alzheimer's disease[J]. PLoS One 15 (3), e0229950.
Liley, D.T., 1997. Spatiotemporal Models in Biological and Artificial Systems. IOS Press, Amsterdam, pp. 89–96.
Malaguarnera, G., Pennisi, M., Bertino, G., et al., 2018. Resveratrol in patients with minimal hepatic encephalopathy[J]. Nutrients 10 (3), 329.
May, E.S., 2012. Modulation of oscillatory alpha activity in the somatosensory system by attention and hepatic encephalopathy.
Patel, N.P., Chafekar, N.D., Sonwane, P.B., 2019. Slowing of Alpha Waves on EEG, an Early Marker of Minimal Hepatic Encephalopathy[J], 1. Informatics Publishing Limited.
Prakash, R., Mullen, K.D., 2010. Mechanisms, diagnosis and management of hepatic encephalopathy[J]. Nat. Rev. Gastroenterol. Hepatol. 7 (9), 515–525.
Rose, C., 2002. Increased extracellular brain glutamate in acute liver failure: decreased uptake or increased release?[J]. Metab. Brain Dis. 17, 251–261.
Saltelli, A., Tarantola, S., Campolongo, F., et al., 2004. Sensitivity Analysis in Practice: A Guide to Assessing Scientific Models[M]. Wiley, New York.
Shayegh, F., Bellanger, J.J., Sadri, S., et al., 2013. Analysis of the behavior of a seizure neural mass model using describing functions[J]. Journal of medical signals and sensors 3 (1), 2.
Song, J.L., Paixao, L., Li, Q., et al., 2019. A novel neural computational model of generalized periodic discharges in acute hepatic encephalopathy[J]. J. Comput. Neurosci. 47, 109–124.
Zhang, P., Zhou, L., Chen, L., et al., 2022. Electroencephalography signatures for hepatic encephalopathy in cirrhosis patients treated with proton pump inhibitors: an exploratory pilot study[J]. Biomedicines 10 (12), 3040.